Solar Energy Materials and Solar Cells 176 (2018) 318–323

Contents lists available at ScienceDirect

Solar Energy Materials and Solar Cells

journal homepage: www.elsevier.com/locate/solmat

# Structure-performance relationship on the asymmetric methoxy substituents of spiro-OMeTAD for perovskite solar cells☆

Ming-Dao Zhang[a,*], Dan-Xia Zhao[a], Li Chen[a], Na Pan[a], Cheng-Yan Huang[a,b], Hui Cao[a,*], Min-Dong Chen[a,*]

[a] Department of Chemistry, School of Environmental Science and Engineering, Jiangsu Key Laboratory of Atmospheric Environment Monitoring and Pollution Control, Nanjing University of Information Science & Technology, Nanjing 210044, China
[b] School of Chemistry & Life Science, Nanjing University Jinling College, Nanjing 210089, Jiangsu, PR China

ARTICLE INFO

*Keywords:*
Energy conversion
Hole-transporting materials
Photovoltaic performance
Solar cells

ABSTRACT

The hole-transporting materials (HTMs) play an important role in energy conversion process of perovskite solar cells (PSCs). Here, two spiro-OMeTAD derivatives, 2,4-spiro-OMeTAD and 3,4-spiro-OMeTAD with asymmetric methoxy substituents, have been designed, synthesized and fully characterized. Optimization of the positions of the two methoxy substituents in each of the quadrants was proved to be able to adjust the electronic and optical properties of the HTMs, as investigated by cyclic voltammetry and UV/vis spectroscopy. In particular, PSC devices based on 2,4-spiro-OMeTAD exhibited highly improved photovoltaic performance showing an overall conversion efficiency of 17.2% with excellent stability, which is higher than that of the device derived from spiro-OMeTAD (15.0%) under the same conditions. Besides, 3,4-spiro-OMeTAD based PSCs only achieved a power conversion efficiency of 9.1%, demonstrating a huge influence of HTM structure on the cell performance.

## 1. Introduction

Organic-inorganic metal halide perovskite solar cells (PSCs) have attracted large attention due to their high power conversion efficiency (PCE) and low cost [1–10]. Typically, the perovskite solar cell is composed of FTO/$TiO_2$/perovskite/HTM/Au (Fig. S1, FTO = fluorine-doped tin oxide, HTM = hole transporting material). The perovskite absorbs sunlight and generates electron-hole pairs, which then transport through $TiO_2$ and HTM, respectively. To date, two different main types of HTMs have been applied including organic [11–15] and inorganic [16–18] p-type semiconductors. Among them, organic HTMs play an important role in high-performance perovskite solar cells due to their versatile molecular structures and excellent photoelectrical properties [19–21].

When used in combination with 2,2',7,7'-tetrakis(N,N-di-*p*-methoxyphenyl-amine)−9,9'-spirobifluorene (spiro-OMeTAD) as the HTM, power conversion efficiency (PCE) of over 15% were obtained under 1 sun (100 mW $cm^{-2}$, simulated) illumination [22–27]. Snaith and coworkers [24] showed a maximum performance of $\eta$ = 15.4%, with an open-circuit voltage ($V_{oc}$) of 1.07 V and a short-circuit current density ($J_{sc}$) of 21.5 mA/$cm^2$, based on $CH_3NH_3PbI_{3-x}Cl_x$ deposited as thin layers with spiro-OMeTAD as the hole conductor. Yang et al. [28] improved power conversion efficiency (PCE) to 19.3% for perovskite solar cells with spiro-OMeTAD as the HTM. Recently, spiro-OMeTAD derivatives were widely studied because of their outstanding performance in perovskite solar cells. Jeon et al. synthesized three spiro-OMeTAD derivatives by changing the position of -OMe substituents of spiro-type arylamine HTMs from para- to meta- and ortho-sites, and they investigated the structure-property relationship in perovskite-based hybrid solar cells [29]. Interestingly, the cell using the ortho-substituted derivative in spiro-OMeTAD showed better performance than the para- and meta-substituted derivatives, with an overall PCE of 16.7% under full sunlight [29]. From the results, we can know that the change of the position of methoxyl affects the highest occupied orbital level and the lowest unoccupied orbital level of spiro-OMeTAD.

In this work, we report the synthesis and characterization of two derivatives of spiro-OMeTAD with asymmetric methoxy substituents and their application in perovskite-based solar cells (Fig. S1). The position of *p*-OMe groups in each of the quadrants of spiro-OMeTAD was replaced with *o*-OMe + *p*-OMe groups as well as *m*-OMe + *p*-OMe substituents to afford 2,4-spiro-OMeTAD and 3,4-spiro-OMeTAD (Fig. 1). The role of the methoxy groups in the spiro-OMeTAD substituents is to adjust the electronic properties of the hole conductor. 2,4-spiro-OMeTAD showed rather better performance than the 3,4-spiro-

☆ Electronic Supplementary Information (ESI) available: Experimental details and additional supplementary figures.

* Corresponding authors.
*E-mail addresses:* matchlessjimmy@163.com (M.-D. Zhang), yccaoh@hotmail.com (H. Cao), chenmd@nuist.edu.cn (M.-D. Chen).

http://dx.doi.org/10.1016/j.solmat.2017.10.014
Received 16 June 2017; Received in revised form 26 September 2017; Accepted 19 October 2017
Available online 04 November 2017
0927-0248/ 

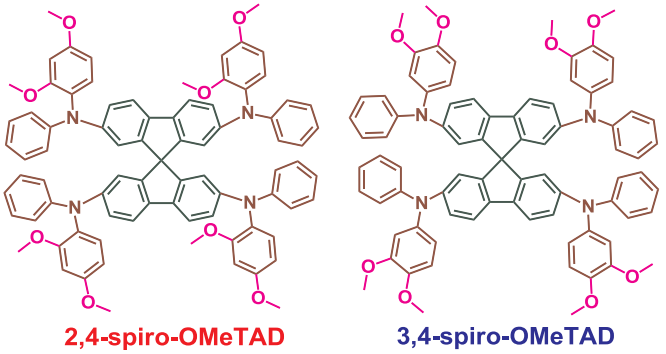


**Fig. 1.** Molecule structures of 2,4-spiro-OMeTAD and 3,4-spiro-OMeTAD.

OMeTAD, with a PCE of 17.2%, a short-circuit current density of 25.6 mA/cm$^2$, an open circuit voltage of 0.956 V, and a fill factor of 0.701 under AM 1.5 G illumination at 100 mW cm$^{-2}$. It is interesting that the perovskite solar cells including 2,4-spiro-OMeTAD as HTM achieves a higher energy conversion efficiency than that of conventional spiro-OMeTAD with an over PCE of 15.0% under the same conditions.

## 2. Experimental

### 2.1. Materials

Spiro-OMeTAD was purchased from Sunlaite Co., Inc. Tris(dibenzylideneacetone)dipalladium(0), tri-*tert*-butylphosphine, 2,2',7,7'-tetra-bromo-9,9'-spirobi[9H-fluorene] and all other chemicals were purchased from HWRK Chemical Co., Ltd. All reagents and solvents were used as received. Methylbenzene was distilled with $CaH_2$. Spiro-OMeTAD derivatives were synthesized by the Buchwald-Hartwig amination reaction, and carried out between 2,2',7,7'-tetrabromo-9,9'-spirobifluorene (**1**) and the respective dimethoxy-diphenylamines containing *o*-OMe and *p*-OMe, or *m*-OMe and *p*-OMe substituents (**2**, **3** respectively). The two spiro-type arylamine derivatives with different substitution positions are denoted as 2,4-spiro-OMeTAD and 3,4-spiro-OMeTAD (**5**, **6** respectively). All the spiro-OMeTAD compounds were purified by column chromatography followed by recrystallization and characterization by $^1$H/$^{13}$C NMR spectroscopy (see the SI). All the analytical data were consistent with the proposed structures. The two compounds have good solubility in all common organic solvents. The synthetic reactions of the spiro-OMeTAD derivatives are shown in Fig. S2.

### 2.2. Syntheses of HTMs

#### 2.2.1. Synthesis of 2,4'-dimethoxy-N-phenylaniline (2)

In a 50 mL two-necked flask, 2,4-dimethoxyaniline (2.00 g, 13.08 mmol), bromobenzene (2.26 g, 14.38 mmol), sodium tert-butoxide (1.88 g, 19.6 mmol), tris(dibenzylideneacetone)dipalladipalladium(0) (0.12 g, 0.13 mmol) and tri-*tert*-butylphosphine (0.042 g, 0.21 mmol) were mixed. Next, 25 mL of anhydrous toluene was added into the flask under a nitrogen atmosphere. The mixture was stirred at 110 °C for 12 h under a nitrogen atmosphere. The solution was cooled down to room temperature and extracted with ethyl acetate and brine water. The organic phase was dried over anhydrous $MgSO_4$. The organic phases were dried using rotary evaporator. Finally, the residue was purified by column chromatography (ethyl acetate/hexane = 1/10) to afford a colorless sticky solid in 49% yield (1.46 g). $^1$H NMR ($CDCl_3$, 400 MHz): δ, [ppm]: 3.84 (s, 3 H), 3.87 (s, 3 H), 6.49 (dd, 1 H, $J_1$ = 4 Hz, $J_2$ = 4 Hz), 6.58 (d, 1 H, $J$ = 4 Hz), 6.89 (t, 1 H, $J_1$ = 8 Hz), 7.03–7.05 (m, 2 H), 7.25–7.29 (m, 3 H).

#### 2.2.2. Synthesis of 3,4'-dimethoxy-N-phenylaniline (3)

In a 50 mL two-necked flask, 3,4-dimethoxyaniline (2.00 g, 13.08 mmol), bromobenzene (2.26 g, 14.38 mmol), sodium tert-butoxide (0.188 g, 19.6 mmol), tris(dibenzylideneacetone)dipalladium(0) (0.12 g, 0.013 mmol) and tri-*tert*-butylphosphine (0.042 g, 0.21 mmol) were mixed. Next, 25 mL of anhydrous toluene was added into the flask under a nitrogen atmosphere. The mixture was stirred at 110 °C for 12 h under a nitrogen atmosphere. The solution was cooled down to room temperature and extracted with ethyl acetate and brine water. The organic phase was dried over anhydrous $MgSO_4$. The organic phases were dried using rotary evaporator. Finally, the residue was purified by column chromatography (ethyl acetate/hexane = 1/10) to afford a colorless sticky solid in 51% yield (1.52 g). $^1$H NMR (DMSO, 400 MHz): δ, [ppm]: 3.86 (s, 3 H), 3.89 (s, 3 H), 5.56 (s, 1 H),6.70 (dd, 1 H, $J_1$ = 2.8 Hz, $J_2$ = 2.8 Hz), 6.75 (d, 1 H, $J$ = 4.2 Hz), 6.84 (d, 1 H, $J$ = 8.8 Hz), 6.88 (t, 1 H, $J$ = 7.6 Hz), 6.97 (d, 2 H, $J$ = 7.6 Hz), 7.26 (m, 2 H).

#### 2.2.3. Synthesis of 2,4-spiro-OMeTAD (5)

In a 50 mL two-necked flask, 2,4'-dimethoxy-N-phenylaniline (**2**) (1.00 g, 4.36 mmol), 2,2',7,7'-tetrabromo,9,9'-spirobi[9H-fluorene] (0.62 g, 0.97 mmol), sodium tert-butoxide (0.56 g, 5.8 mmol), tris(dibenzylideneacetone)dipalladium(0) (0.035 g, 0.039 mmol) and tri-*tert*-butylphosphine (0.012 g, 0.06 mmol) were mixed. Next, 15 mL of anhydrous toluene was added into the flask under a nitrogen atmosphere. The mixture was stirred at 110 °C for 12 h under a nitrogen atmosphere. The solution was cooled down to room temperature and extracted with ethyl acetate and brine water. The organic phase was dried over anhydrous $MgSO_4$. The organic phases were dried using rotary evaporator. Finally, the residue was purified by column chromatography (ethyl acetate/hexane = 1/2) to afford a beige solid in 45% yield (0.54 g). $^1$H NMR ($CDCl_3$, 400 MHz, Fig. S3): δ, [ppm]: 3.51 (s, 12 H), 3.83 (s, 12 H), 6.47 (m, 8 H), 6.69 (s, 4 H), 6.77 (m, 12 H), 6.90 (d, 4 H, $J$ = 7.2 Hz), 7.01 (d, 4 H, $J$ = 8 Hz), 7.08 (m, 8 H), 7.44 (d, 4 H, $J$ = 6.8 Hz). $^{13}$C NMR ($CDCl_3$, 100 Hz, Fig. S4): δ, [ppm]: 55.45, 55.71, 65.68, 100.68, 105.20, 118.61, 118.87, 119.74, 122.90, 128.56, 130.45, 136.19, 146.28, 148.24, 149.89, 156.94, 158.69. The FT-IR spectrum of 2,4-spiro-OMeTAD is shown in Fig. S5.

#### 2.2.4. Synthesis of 3,4-spiro-OMeTAD (6)

In a 50 mL two-necked flask, 3,4'-dimethoxy-N-phenylaniline **(3)** (1.00 g, 4.36 mmol), 2,2',7,7'-tetrabromo,9,9'-spirobi[9H-fluorene] (0.62 g, 0.97 mmol), sodium tert-butoxide (0.56 g, 5.8 mmol), tris(dibenzylideneacetone)dipalladium(0) (0.035 g, 0.039 mmol) and tri-*tert*-butylphosphine (0.012 g, 0.06 mmol) were mixed. Next, 15 mL of anhydrous toluene was added into the flask under a nitrogen atmosphere. The mixture was stirred at 110 °C for 12 h under a nitrogen atmosphere. The solution was cooled down to room temperature and extracted with ethyl acetate and brine water. The organic phase was dried over anhydrous $MgSO_4$. The organic phases were dried using rotary evaporator. Finally, the residue was purified by column chromatography (ethyl acetate/hexane = 1/2) to afford a beige solid in 45% yield (0.53 g). $^1$H NMR ($CDCl_3$, 400 MHz, Fig. S6): δ, [ppm]: 3.72 (s, 12 H), 3.90 (s, 12 H), 6.58 (d, 4 H, $J$ = 8 Hz), 6.68 (s, 4 H), 6.74 (s, 4 H), 6.79 (d, 4 H, $J$ = 8.8 Hz), 6.95 (m, 8 H), 6.98 (m, 8 H), 7.21 (t, 8 H, $J$ = 6.8 Hz), 7.50 (d, 4 H, $J$ = 8 Hz). $^{13}$C NMR ($CDCl_3$, 100 Hz, Fig. S7): δ, [ppm]: 56.01, 56.16, 65.76, 109.48, 111.94, 117.37, 118.92, 120.27, 121.60, 122.14, 123.81, 128.99, 136.22, 141.02, 145.62, 146.77, 148.10, 149.61, 149.66. The FT-IR spectrum of 3,4-spiro-OMeTAD is shown in Fig. S5.

### 2.3. Measurements

#### 2.3.1. UV−Vis Absorption, Electrochemical Measurement, and Fluorescent

$^1$H and $^{13}$C NMR spectra were measured using Bruker 400 MHz FT NMR and 500 NMR spectrometers. Ultraviolet-visible (*UV–vis*)